

Article

Anion Coordination Improves High-Temperature Performance and Stability of NaPF₆-Based Electrolytes for Supercapacitors

J. Landon Tyler¹, Robert L. Sacchi^{2,*}  and Jagjit Nanda^{2,*}¹ Bredesen Center, University of Tennessee, Knoxville, TN 37996, USA; jtyler9@vols.utk.edu² Chemical Sciences Division, Oak Ridge National Laboratory, Oak Ridge, TN 37830, USA

* Correspondence: saccir1@ornl.gov (R.L.S.); nandaj@ornl.gov (J.N.)

Abstract: Electrolyte stability can be improved by incorporating complexing agents that bind key decomposition intermediates and slow down decomposition. We show that hexamethylphosphoramide (HMPA) extends both the thermal stability threshold of sodium hexafluorophosphate (NaPF₆) in dimethoxyethane (DME) electrolyte and the cycle life of double-layer capacitors. HMPA forms a stable complex with PF₅, an intermediate in PF₆ anion thermal degradation. Unbound, this intermediate leads to autocatalytic degradation of the electrolyte solution. The results of electrochemical impedance spectroscopy (EIS) and galvanostatic cycling measurements show large changes in the cell without the presence of HMPA at higher temperatures (≥ 60 °C). Fourier transform infrared spectroscopy (FTIR) on the liquid and gas phase of the electrolyte shows without HMPA the formation of measurable amounts of PF₅ and HF. The complimentary results of these measurements proved the usefulness of using Lewis bases such as HMPA to inhibit the degradation of the electrolyte solution at elevated temperatures and potentially lead to improve cycle life of a nonaqueous capacitor. The results showed a large increase in capacitance retention during cycling (72% retention after 750,000 cycles). The results also provide evidence of major decomposition processes (0% capacitance retention after 100,000 cycles) that take place at higher temperatures without the additive of a thermal stability additive such as HMPA.

Keywords: Na-ion electrolytes; supercapacitors; high-temperature electrolyte

Citation: Tyler, J.L.; Sacchi, R.L.; Nanda, J. Anion Coordination Improves High-Temperature Performance and Stability of NaPF₆-Based Electrolytes for Supercapacitors. *Energies* **2021**, *14*, 4409. <https://doi.org/10.3390/en14154409>

Academic Editor: Changhong Wang

Received: 9 June 2021

Accepted: 8 July 2021

Published: 21 July 2021

Publisher's Note: MDPI stays neutral with regard to jurisdictional claims in published maps and institutional affiliations.



Copyright: © 2021 by the authors. Licensee MDPI, Basel, Switzerland. This article is an open access article distributed under the terms and conditions of the Creative Commons Attribution (CC BY) license (<https://creativecommons.org/licenses/by/4.0/>).

1. Introduction

Energy storage devices have taken on a monotonous variety of forms (fuel cells, capacitors, batteries, etc.) to satisfy numerous operating conditions: energy density, voltage windows, cycle rate, power density, high temperature ranges, et cetera [1–5]. Commercial supercapacitors or electric double-layer capacitors (EDLC) generally have lower energy densities but higher power densities compared to Li-ion batteries, 10 vs. 200 Wh kg⁻¹, and 10⁴ vs. 10² W kg⁻¹ [1,6–11], respectively. Unlike batteries, supercapacitors do not utilize the Faradaic redox process to store charge in the bulk of the materials; rather, they store charge along the electric double layer (surface) of pores within high surface area electrode materials. Double-layer charging is fast, which enables supercapacitors to have excellent power (rate) performance and long cycle life (>10⁶ cycles) at the cost of poor energy density. As such, EDLCs are used for cold start assists for generators and memory back-up, as well as to deliver high power for smart grids, transport, and aerospace applications [10–12]. Aqueous-based EDLC are limited to 1.2 V due to the electrochemical window of water. The maximum energy stored (W) within capacitors is directly related to the specific capacitance (C) and the voltage window of the system (V) as follows:

$$W = \frac{1}{2}CV^2 \quad (1)$$

Equation (1) suggests that increasing the working voltage of the electrolyte will dramatically improve the amount of stored energy. Nonaqueous EDLC electrolytes

have been developed based on acetonitrile and propylene carbonate as solvent systems. These electrolytes were shown to increase energy stored, at the expense, however, of the power [6,9,13,14]. Clearly, successful development of new electrolyte compositions needs optimization of a number of materials, as well as electrochemical properties such as working potential window, cycling rate, compatible carbon and binder systems, and other factors. Operating temperature is also an important factor as some electrolytes are unstable at temperatures above 60 °C. This instability leads to the creation of byproducts that inevitably increase the effective series resistance (ESR), reduce the operating voltage and power, and may cause cell pressure build-up. Another major issue is the corrosion of the current collector (aluminum) at higher oxidation potential and instability of the binder material, Teflon, at voltages <1 V. Simply put, these issues not only result in lower performance, device failure, and dangerous conditions, but can cause high pressure build-up, open flames, leakage of toxic chemicals, and fumes [9,15,16].

Our group has shown that sodium hexafluorophosphate (NaPF₆) and the monoglyme (dimethoxyethane, DME) electrolyte possess a 3.5 V electrochemical window. This window approximately doubles the energy density typically found with ACN-based electrolytes, which are limited to ~2.5 V [6]. DME-based electrolytes have low viscosity, which implies higher ionic conductivity (power density) [17–21]. The PF₆[−] anion is commonly used in commercial nonaqueous electrolytes because it passivates the surface of the aluminum against corrosion, which is the standard current collector in EDLC and lithium-ion batteries [22–25]. However, PF₆-based electrolytes are unstable above 60 °C because they decompose to PF₅, which then promotes an autocatalytic decomposition reaction that will continue until all the PF₆[−] is consumed [26–28]. Li et al. reported that using Lewis bases such as pyridine, hexamethoxycyclotriphosphazene (HMOPA), and hexamethylphosphoramide (HMPA) in LiPF₆-carbonate-based electrolyte greatly improves the thermal stability of the electrolyte by complexing with PF₅. The Lewis-base–PF₅ complex inhibits the autocatalytic decomposition reaction [15–28]. It is important to note that adding additives to electrolyte solutions can change the properties of the bulk solution including voltage windows.

In this study, we build upon previous reports [15,28] and demonstrate that the thermal management additive, HMPA, also improves the stability of NaPF₆ salt in glyme-based solvents without compromising device performance. Specifically, we performed electrochemical impedance spectroscopy (EIS) to monitor the thermal decomposition (degradation) of the electrolyte by observing increases in the overall resistance of the cell and corresponding changes in capacitive behavior. We further performed Fourier transform infrared spectroscopy (FTIR) on both the solution and gas phase of the electrolyte to better understand the inhibition of electrolyte decomposition. The gas-phase IR spectra provides evidence of the formation of PF₅ gas without the HMPA, but these peaks do not exist in the presence of HMPA. Our results provide evidence that HMPA can be used as an additive to increase the thermal stability of NaPF₆ in DME at elevated temperatures (>60 °C). Based on these observations, we propose a simplistic pathway on how the HMPA–PF₅ complex inhibits the autocatalytic decomposition reaction as reported in other systems [15,28] and improves cycle life and performance.

2. Materials and Methods

Electrolyte preparation: Electrolytes were prepared in an argon-filled glovebox. Before mixing, DME and HMPA were dried over a 4A molecular sieve. NaPF₆ (98%, Sigma Aldrich) was dissolved into DME (battery grade, Mitsubishi Chemical Company) to give a 1 molal solution (1 mol NaPF₆/1 kg of DME). The electrolyte was stored over sodium to remove impurities for at least one week. HMPA (Sigma Aldrich) was added to the electrolyte solution prior to testing in specified amounts—typically 20% by weight of the solution. It is important to note that HMPA cannot be in the presence of sodium metal as it will violently react.

Electrode preparation: The carbon electrodes were prepared from ultrasonicated aqueous slurries containing Black Pearls 2000 (BP2000, Cabot Corporation, Boston, MA, USA, BET surface area: around 1460 m²/g) with carboxymethyl cellulose (CMC, Sigma Aldrich, St. Louis, MO, USA, molecular weight 700,000) as a binder. The electrode slurry was made by tape casting 85% BP2000 and 15% CMC onto an aluminum current collector. The electrodes were dried at 120 °C under vacuum. The weight balance between the two electrodes is 1 to 1.

Electrochemical measurements: Two electrode button cells (316 L stainless steel, CR2032, Hohsen Corp., Osaka, Japan) containing two carbon electrodes and a Celgard separator (2325) were used for all measurements. All impedance measurements were made in the frequency range of 20 kHz to 10 mHz and acquired using Bio-Logic instruments (VSP3). The tests were performed at elevated temperatures and were controlled in a Cincinnati Sub Zero temperature chamber. Galvanic cycling measurements were performed between 0 and 1 V or 3 V at 5 mA using Bio-Logic instruments (VSP3). Cyclic voltammetry was performed at 10 mV/s.

Characterization: The infrared spectroscopy spectra of the solution was measured using a diamond attenuated total reflection accessory (ATR) attached to a Bruker ALPHA FTIR spectrometer within an argon-filled glovebox. Gas-phase FTIR (Cary 680 FTIR, Agilent Technologies, Santa Clara, CA, USA) spectra were measured every 3 min over 15 h inside a gas cell specifically made for studying gaseous products without interference from the ambient atmosphere as seen in Figure A1. The cell was purged with helium and then sealed from the environment using Viton gaskets and KBr windows. The cell was sealed with KBr windows and wrapped in a heating coil and heated to 85 °C.

3. Results and Discussion

Cyclic voltammetry was performed to establish the electrochemical stability window of the electrolyte. Figure 1a,b shows that the voltage window is much smaller in the presence of HMPA of around 2.5 V (green curve, Figure 1b) versus the 3 V of the HMPA-free electrolyte 2.8 V (purple curve, Figure 1a). Though the voltage window is lower, cycling at 80 °C at both 1V and 3V show a remarkable difference in cycling performance. Without HMPA, the capacitance of the cell quickly drops from around 50 to ~0 F/g, which can be corroborated by the EIS measurements taken after 5000 cycles, which show significant increase in cell resistance (7 to 150 Ω at the end of the semicircle). We attribute these changes to electrolyte breakdown and the passivation of the carbon surface. A similar effect on high-voltage, high-temperature cycling is seen in the HMPA-bearing electrolyte—specifically, the capacitance decays from around 50 to 35 F/g after 25,000 cycles. This shows that in addition to impeding electrolyte decomposition at 80 °C, HMPA limits the destructive effect of high-voltage cycling. The impedance measurements in Figure 1e,f suggest that HMPA prevents surface passivation as the cell impedance (the semicircle in the Nyquist plots) growth is much slower (50 Ω) than without HMPA (150 Ω). Given that cycling at 3 V induces electrochemical degradation, all measurements beyond this point were performed at 1 V and focus solely on the thermal chemical degradation of the electrolyte.

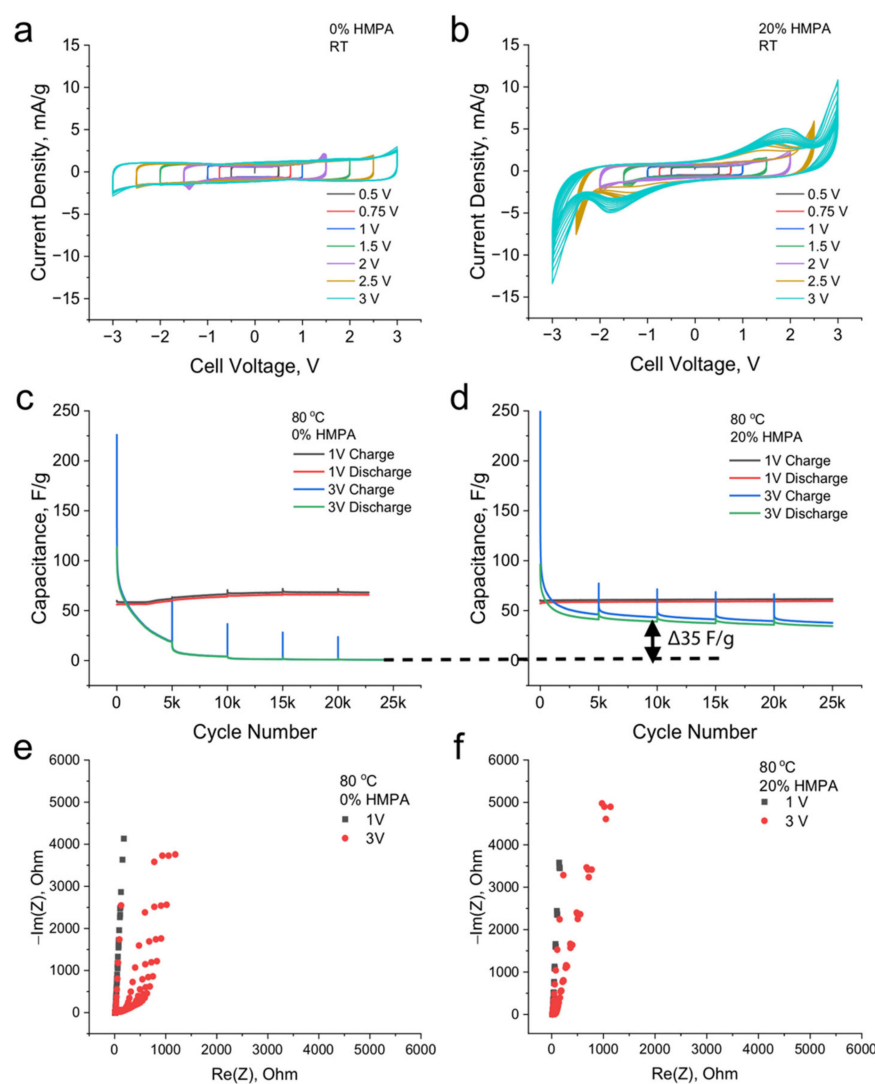


Figure 1. The cyclic voltammetry of 1m NaPF₆ without HMPA (a) and with HMPA (b). The galvanostatic cycling measurements of 1m NaPF₆ in DME without HMPA (c) and with HMPA (d) at 5 mA at 80 °C. The spike in capacitance is an artifact from performing EIS at OCV before every 5000 cycles and normalizes after 500 cycles. The Nyquist plots of cells were taken every 5000 cycles without HMPA (e) and with HMPA (f). An increase of around 40 F/g of stable cycling can be observed with the addition of HMPA at 80 °C and cycling at 3 V.

EIS measurements were performed to verify ideal capacitive behavior in the cells for this study. The low frequency region shown in Nyquist plots should be parallel with the imaginary axis for an ideal capacitor [13,29]. Deviation from this ideality can be attributed to surface roughness, adsorption processes, and side reactions with the electrolyte [30]. With that said, near-ideal capacitive behavior in the EIS measurements was found when the cell voltage was kept between 0 and 1 V with and without HMPA—Figure 2a,b. The figures also show that the addition of HMPA did not affect the room temperature impedance except in small deviation of capacitance, though ideal capacitive behavior was observed. Room temperature galvanostatic cycling was performed to measure the cycling performance of cells containing 0% and 20% HMPA by weight. During cycling, the EIS measurements performed every 1000 cycles show no change in capacitive behavior at well over 200,000 cycles—see Figure 2c,d. The specific capacitance is retained with a 99% retention over 200,000 cycles as shown in Figure 2e,f. This provided evidence that the addition of HMPA does not cause a detrimental effect on the cycling performance of the electrolyte.

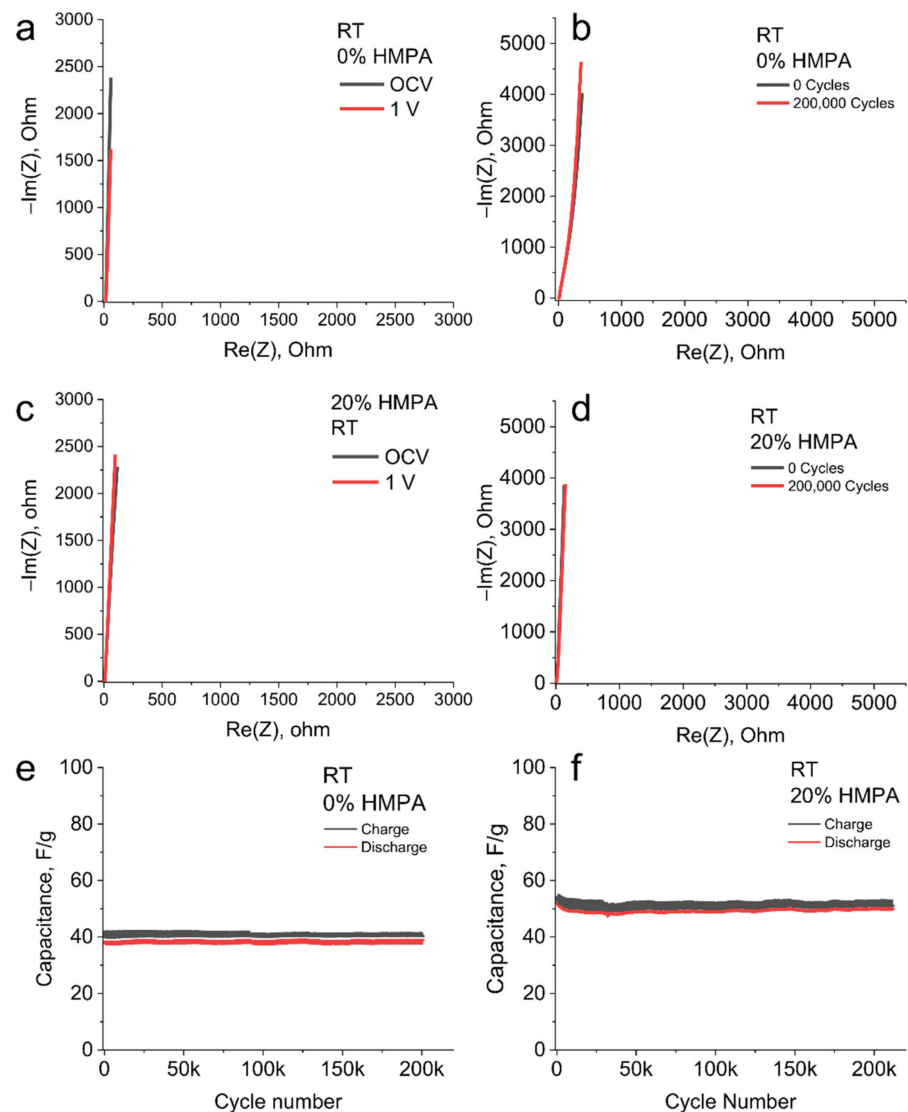


Figure 2. Nyquist plot without (a) and with HMPA (b) at room temperature. EIS measurements taken during galvanostatic cycling without (c) and with HMPA (d). Galvanic cycling capacitance vs. cycling number plots without (e) and with (f) HMPA.

The impedance of the cells was measured periodically during cycling (every 1000 cycles) to track changes in the capacitive behavior of the cell. The cells underwent testing at 80 °C after being equilibrated for at least 1 h. The cells were then cycled between 0 and 1 V, while an impedance measurement was taken every 5000 cycles. Without HMPA, a noticeable growth in a semicircle in the high-frequency domain indicates a possible passivation of the electrode surface. This would lead to a decrease in capacitance while cycling, which can be observed in Figure 3b. The cell is essentially dead after 60,000 cycles after a quick decrease in capacitance. The cell continued cycling for 1,000,000 cycles without any change in capacitance, but a larger growth in passivation on the surface. The addition of HMPA lead to stable cycling over 739,000 cycles at 80 °C—see Figure 3c,d. The EIS measurements also showed no significant change in impedance during cycling. There was slight fading with each cycle, but this electrode and electrolyte composition was not optimized, as it falls outside the focus of this study. These results provided evidence that the addition of HMPA led to longer cycle life at elevated temperatures.

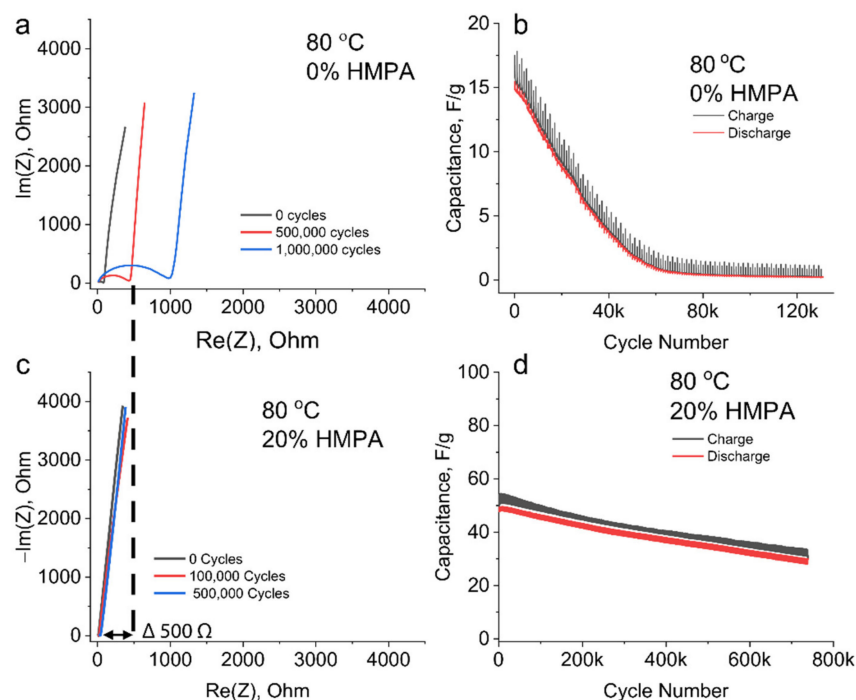


Figure 3. Electrochemical data of cells without HMPA at 80 °C; (a) representative impedance data; (b) galvanic cycling data at 5 mA. There is clear evidence of cell degradation without the addition of HMPA. (c) Representative impedance data with 20% by wt. HMPA at 80 °C; (d) galvanic cycling data (The spikes in the data are an artifact of how the data is taken. They occur after every EIS measurement). Note also that the initial capacitance of cells without HMPA at 80 °C vary due to unaccounted for degradation while equilibrating at 80 °C.

Visual evidence to the improved thermal stability brought on by HMPA is shown in Figure A2. Here, the addition of 5% and 10% of HMPA keeps the electrolyte from turning dark brown after 40 h of heating at 85 °C. The mechanism for increasing the thermal stability of PF₆-based electrolytes includes scavenging PF₅ or acidic byproducts. An equilibrium is suspected to develop between PF₆[−] and PF₅ in the solution phase [15].



This equilibrium is disrupted, and the reaction shifts towards the formation of PF₅ at higher temperatures and begins the process of continual electrolyte degradation. In a typical lithium-ion battery electrolyte, PF₅ reacts with impurities found within the cell, including trace water in the electrolyte solution, surface impurities of the electrode, and the solvent of the electrolyte [15]. The plausible decomposition pathway for NaPF₆ in DME is shown in Figure 4. The reaction products are primarily a combination of hydrofluoric acid, POF₃, fluorine containing organic compounds, and carbon dioxide. The reaction is considered autocatalytic since PF₅ will also react with products from its own decomposition pathway as shown in Figure 4. The decomposition pathway shows a large combination of possible products that can be consumed to further the decomposition of the electrolyte. The decomposition products could also act as reactants for surface passivation of the carbon electrodes leading to the loss of capacitance. This phenomenon was measured in Figure 3a, which shows a large increase in resistance with continuous exposure to elevated temperatures. The reaction pathway also highlights that all components of the electrolyte solution are affected by the presence of PF₅. The more important factor is that as PF₅ reacts, it disrupts the equilibrium and results in more PF₅ forming and further degradation of the electrolyte solution in the cell.

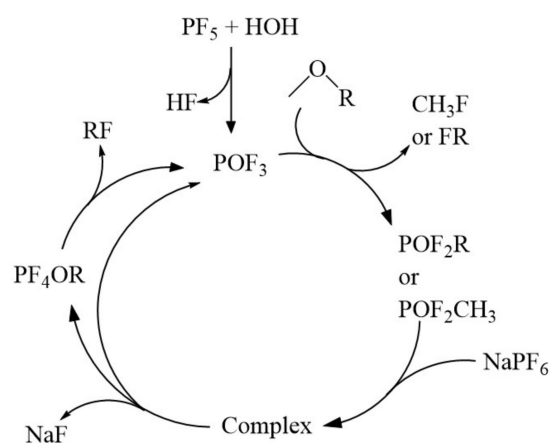


Figure 4. Possible autocatalytic decomposition pathway for NaPF_6 in DME without complexing agents.

On the contrary, HMPA binds with PF_5 , as shown in Figure 5, and forms a highly stable complex. The kinetics of this complexation are thought to be rapid, as PF_5 is unable to induce the autocatalytic decomposition of PF_6^- and other electrolyte species. As with many sacrificial additives, there is a limit to the amount or quantity of HMPA in the electrolyte that can suppress the formation of PF_5 . When all the HMPA in the system is utilized, NaPF_6 thermal degradation resumes [28]. The scope of the paper is not to optimize the necessary amount of HMPA for sodium supercapacitors, but to prove the concept of using a Lewis base such as HMPA as an additive for inhibiting the thermal degradation of NaPF_6 .

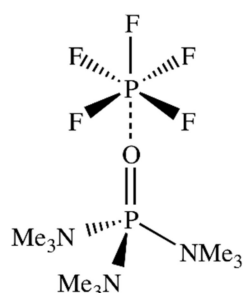


Figure 5. The complex structure between HMPA and PF_5 that may function to prevent thermal decomposition.

FTIR was used to track the decomposition reactions within the electrolytes with and without HMPA added—see Figure 6. The peak at 807 cm^{-1} corresponds to the asymmetric P-F stretching band of the PF_6^- anion, and the peaks centered at about 1087 and 1110 cm^{-1} correspond with the C-O stretching of DME [31]. Signals from HMPA are at 740 , 985 , 1200 , and 1295 cm^{-1} . The relative intensity between 807 and 1087 cm^{-1} drastically decreases after 24 h at $85\text{ }^\circ\text{C}$ without HMPA—see Figure 6a. This decrease indicates a decomposition of PF_6^- . The same bands show little change when 20% HMPA is present—see Figure 6b. This could be because PF_5 exists as a gas at room temperature. To discern the formation of PF_5 , FTIR was performed on the gases evolving from the electrolyte solution at $85\text{ }^\circ\text{C}$ —see Figure 7. After 7 h of exposure, new peaks at 480 and 735 cm^{-1} appear, which are attributed to the P-F stretching bonds of PF_5 [32]. Another notable feature is the generation and consumption of HF corresponding to the peaks between 3600 – 4000 cm^{-1} —see Figure 7b. After 7 h, these peaks begin to diminish which is representative of consumption due to the previously discussed decomposition pathway. Both HF and PF_5 are typical decomposition products of LiPF_6 in organic solvents [33,34].

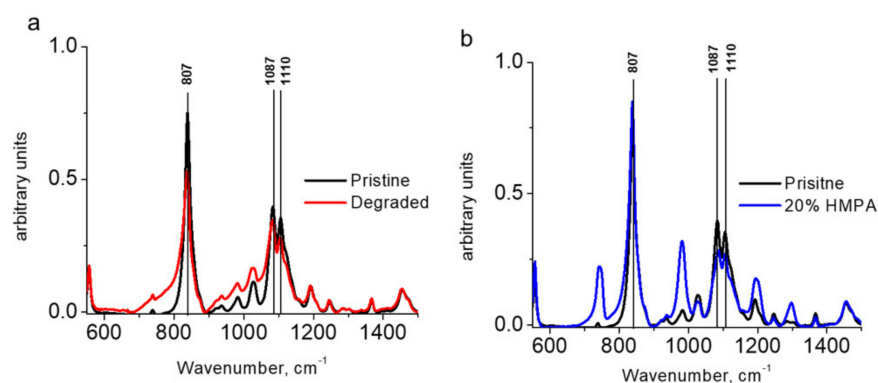


Figure 6. (a) FTIR spectra 1 M NaPF₆ in DME before and after decomposition at 85 °C; (b) FTIR spectra of 1 m NaPF₆ in DME after exposure to 85 °C (compared to pristine 1 m NaPF₆ in DME). Liquid-phase FTIR shows changes in peak intensity of the PF₆ P-F stretch (807 cm⁻¹).

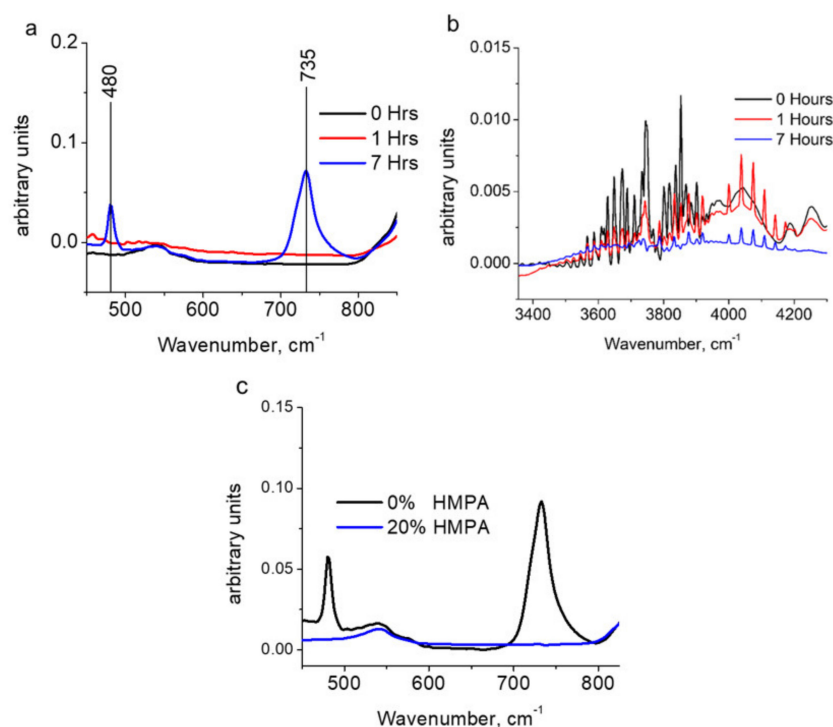


Figure 7. FTIR spectra of gas phase of 1 M NaPF₆ in DME at 85 °C. Top spectra are without HMPA, with (a) highlighting the HF region, (b) highlighting the PF₅ region during degradation, and (c) comparing the effect of HMPA addition after 7 h. NaPF₆ will degrade into PF₅ and HF. HMPA suppresses PF₅ formation in the gas phase.

Neither of these compounds are observed in the FTIR spectra for electrolyte solutions containing HMPA—see Figure 7c. The gas-phase FTIR provides evidence that without HMPA, the electrolyte solution degraded and formed PF₅ gas. The correlation of the lack of degradation of NaPF₆ in the liquid phase and the absence of the formation of PF₅ in the gas phase means that HMPA complexed with PF₅. This complexation led to inhibition of the degradation reaction and stability of the electrolyte at higher temperatures.

4. Conclusions

Electrochemical and infrared spectroscopy provided evidence that without HMPA, fluorophosphate-based electrolytes undergo rapid thermal degradation. FTIR results indicate that PF₆⁻ undergoes thermal breakdown into PF₅ and HF. With the addition of HMPA, EDLC cells retained their capacitive behavior and showed stable cycling performance at

elevated temperatures. Here, no major changes in the FTIR spectra were observed. Our results support the notion that HMPA complexes with PF_5 in a similar manner as that previously hypothesized in Li-ion systems. Similar research could be performed pairing Lewis bases with other PF_6 -based or Lewis acid anion salts for a myriad of applications and working temperatures. This provides one possible avenue for the development of PF_6 -based supercapacitors for high-temperature applications.

Author Contributions: All authors participated in the conceptualization, methodology, analysis, and writing of this manuscript. J.L.T. lead the investigation data curation and original draft preparation. Supervision was supplied by J.N. and R.L.S. All authors have read and agreed to the published version of the manuscript.

Funding: This research received no external funding.

Institutional Review Board Statement: Not applicable.

Informed Consent Statement: Not applicable.

Data Availability Statement: The data presented in this study are available on request from the corresponding author.

Acknowledgments: J.L.T. and J.N. acknowledge support from Energy Storage program, Office of Electricity, Department of Energy. R.L.S. (FTIR and analysis) was supported by the Fluid Interface Reactions, Structures and Transport (FIRST) Center, an Energy Research Center funded by the U.S. Department of Energy, Office of Science, Office of Basic Energy Science.

Conflicts of Interest: The authors declare no conflict of interest. The funders had no role in the design of the study; in the collection, analyses, or interpretation of data; in the writing of the manuscript, or in the decision to publish the results.

Appendix A

Figure A1 shows the typical setup used for the in situ gas-phase FTIR that was used for this experiment. The sample is placed inside the cell while the different values across the top were used to outgas and replace air within the cell with inert gases such as helium and argon.

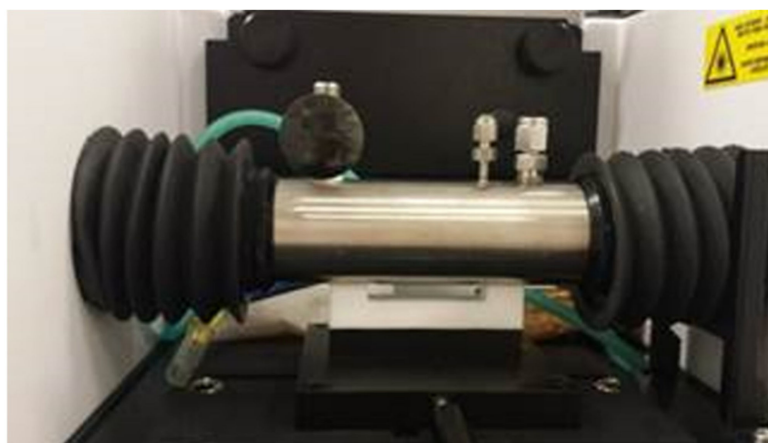


Figure A1. Gas cell used for gas-phase FTIR measurements.

Figure A2 shows that the electrolyte leads to certain degradation unless an adequate amount of HMPA is added to the electrolyte. One noticeable feature is that a small amount of HMPA is enough to prolong the decomposition of the electrolyte.

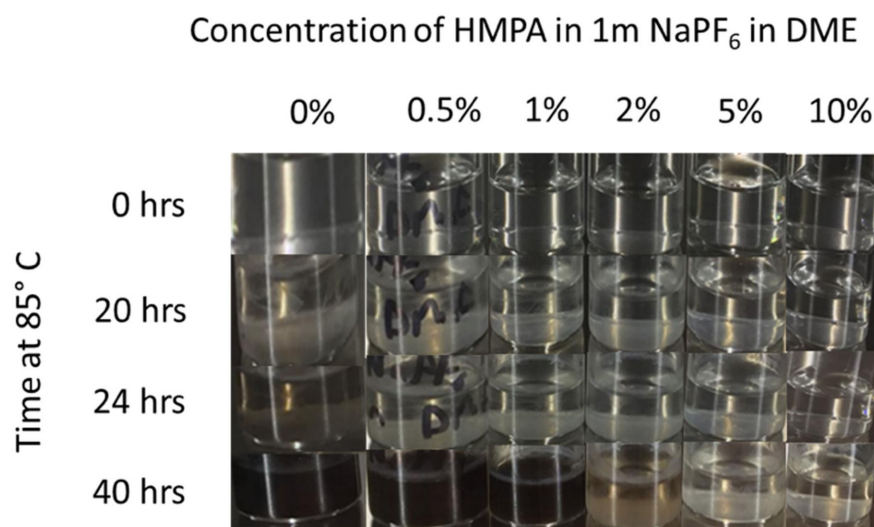


Figure A2. Visual degradation of NaPF₆ in DME with varying concentrations of HMPA at 85 °C.

References

- Winter, M.; Brodd, R.J. What are batteries, fuel cells, and supercapacitors? *Chem. Rev.* **2004**, *104*, 4245–4269. [[CrossRef](#)]
- Liu, C.; Yu, Z.; Neff, D.; Zhamu, A.; Jang, B.Z. Graphene-Based Supercapacitor with an Ultrahigh Energy Density. *Nano Lett.* **2010**, *10*, 4863–4868. [[CrossRef](#)] [[PubMed](#)]
- Zhang, S.S. A review on electrolyte additives for lithium-ion batteries. *J. Power Sources* **2006**, *162*, 1379–1394. [[CrossRef](#)]
- Hu, M.; Pang, X.; Zhou, Z. Recent progress in high-voltage lithium ion batteries. *J. Power Sources* **2013**, *237*, 229–242. [[CrossRef](#)]
- Scrosati, B.; Garche, J. Lithium batteries: Status, prospects and future. *J. Power Sources* **2010**, *195*, 2419–2430. [[CrossRef](#)]
- Ruther, R.E.; Sun, C.-N.; Holliday, A.; Cheng, S.; Delnick, F.M.; Zawodzinski, T.A.; Nanda, J. Stable Electrolyte for High Voltage Electrochemical Double-Layer Capacitors. *J. Electrochem. Soc.* **2017**, *164*, A277–A283. [[CrossRef](#)]
- Balducci, A.; Dugas, R.; Taberna, P.L.; Simon, P.; Pl, D. High temperature carbon—Carbon supercapacitor using ionic liquid as electrolyte. *J. Power Sources* **2007**, *165*, 922–927. [[CrossRef](#)]
- Yan, J.; Wang, Q.; Wei, T.; Fan, Z. Recent Advances in Design and Fabrication of Electrochemical Supercapacitors with High Energy Densities. *Adv. Energy Mater.* **2014**, *4*, 1300816. [[CrossRef](#)]
- Béguin, F.; Presser, V.; Balducci, A.; Frackowiak, E. Carbons and Electrolytes for Advanced Supercapacitors. *Adv. Mater.* **2020**, *26*, 2219–2251. [[CrossRef](#)]
- Conte, M. Supercapacitors Technical Requirements for New Applications. *Fuel Cells* **2010**, *10*, 806–818. [[CrossRef](#)]
- Kanchev, H.; Lu, D.; Colas, F.; Lazarov, V.; Francois, B. Energy Management and Operational Planning of a Microgrid with a PV-Based Active Generator for Smart Grid Applications. *IEEE Trans. Ind. Electron.* **2011**, *58*, 4583–4592. [[CrossRef](#)]
- Hung, K.; Masarapu, C.; Ko, T.; Wei, B. Wide-temperature range operation supercapacitors from nanostructured activated carbon fabric. *J. Power Sources* **2009**, *193*, 944–949. [[CrossRef](#)]
- Rafik, F.; Gualous, H.; Gallay, R.; Crausaz, A.; Berthon, A. Frequency, thermal and voltage supercapacitor characterization and modeling. *J. Power Sources* **2007**, *165*, 928–934. [[CrossRef](#)]
- Jian-wen, L.I.U.; Xin-hai, L.I.; Zhi-Xing, W. Preparation and characterization of lithium hexafluorophosphate for lithium-ion battery electrolyte. *Trans. Nonferr. Met. Soc. China* **2010**, *20*, 344–348. [[CrossRef](#)]
- Li, W.; Campion, C.; Lucht, B.L.; Ravdel, B.; Dicarolo, J.; Abraham, K.M. Additives for Stabilizing LiPF₆-Based Electrolytes Against Thermal Decomposition. *J. Electrochem. Soc.* **2005**, *152*, 1361–1365. [[CrossRef](#)]
- Zhang, L.L.; Zhao, X.S. Carbon-based materials as supercapacitor electrodes. *Chem. Soc. Rev.* **2009**, *38*, 2520–2531. [[CrossRef](#)] [[PubMed](#)]
- Borodin, O.; Behl, W.; Jow, T.R. Oxidative Stability and Initial Decomposition Reactions of Carbonate, Sulfone, and Alkyl Phosphate-Based Electrolytes. *J. Phys. Chem. C* **2013**, *117*, 8661–8682. [[CrossRef](#)]
- Chiba, K.; Ueda, T.; Yamaguchi, Y.; Oki, Y.; Shimodate, F.; Naoi, K. Electrolyte Systems for High Withstand Voltage and Durability I. Linear Sulfones for Electric Double-Layer Capacitors. *J. Electrochem. Soc.* **2011**, *158*, A872–A882. [[CrossRef](#)]
- Brandt, A.; Isken, P.; Lex-Balducci, A.; Balducci, A. Adiponitrile-based electrochemical double layer capacitor. *J. Power Sources* **2012**, *204*, 213–219. [[CrossRef](#)]
- Brandt, A.; Balducci, A. The Influence of Pore Structure and Surface Groups on the Performance of High Voltage Electrochemical Double Layer Capacitors Containing Adiponitrile-Based Electrolyte. *J. Electrochem. Soc.* **2012**, *159*, A2053–A2059. [[CrossRef](#)]
- Morales, D.; Ruther, R.E.; Nanda, J.; Greenbaum, S. Ion transport and association study of glyme-based electrolytes with lithium and sodium salts. *Electrochim. Acta* **2019**, *304*, 239–245. [[CrossRef](#)]

22. Yang, H.; Kwon, K.; Devine, T.M.; Evans, J.W. Aluminum Corrosion in Lithium Batteries an Investigation Using the Electrochemical Quartz Crystal Microbalance. *J. Electrochem. Soc.* **2000**, *147*, 4399–4407. [[CrossRef](#)]
23. Zhang, S.S.; Jow, T.R. Aluminum corrosion in electrolyte of Li-ion battery. *J. Power Sources* **2002**, *109*, 458–464. [[CrossRef](#)]
24. Vali, R.; Janes, A.; Lust, E. Vinylene Carbonate as Co-Solvent for Low-Temperature Mixed Electrolyte Based Supercapacitors. *J. Electrochem. Soc.* **2016**, *163*, A851–A857. [[CrossRef](#)]
25. Laheäär, A.; Jänes, A.; Lust, E. NaClO₄ and NaPF₆ as potential non-aqueous electrolyte salts for electrical double layer capacitor application. *Electrochim. Acta* **2012**, *82*, 309–313. [[CrossRef](#)]
26. Campion, C.L.; Li, W.; Lucht, B.L. Thermal Decomposition of LiPF₆-Based Electrolytes for Lithium-Ion Batteries. *J. Electrochem. Soc.* **2005**, *152*, 2327–2334. [[CrossRef](#)]
27. Okamoto, Y. Ab Initio Calculations of Thermal Decomposition Mechanism of LiPF₆-Based Electrolytes for Lithium-Ion Batteries. *J. Electrochem. Soc.* **2013**, *160*, 404–409. [[CrossRef](#)]
28. Campion, C.L.; Li, W.; Euler, W.B.; Lucht, B.L.; Ravdel, B.; Dicarolo, J.F.; Gitzendanner, R.; Abraham, K.M. Suppression of Toxic Compounds Produced in the Decomposition of Lithium-Ion Battery Electrolytes. *Electrochem. Solid-State Lett.* **2004**, *7*, 194–197. [[CrossRef](#)]
29. Taberna, P.L.; Simon, P.; Fauvarque, J.F. Electrochemical Characteristics and Impedance Spectroscopy Studies of Carbon-Carbon Supercapacitors. *J. Electrochem. Soc.* **2003**, *153*, 292–300. [[CrossRef](#)]
30. Bohlen, O.; Kowal, J.; Sauer, D.U. Ageing behaviour of electrochemical double layer capacitors Part I. Experimental study and ageing model. *J. Power Sources* **2007**, *172*, 468–475. [[CrossRef](#)]
31. Goren, E.; Chusid, O.; Aurbach, D. The Application of In SITU FTIR Spectroscopy to the Study of Surface Films Formed on Lithium and Noble Metals at Low Potentials in Li Battery Electrolytes. *J. Electrochem. Soc.* **1991**, *138*, 6–9. [[CrossRef](#)]
32. Lugez, C.L.; Irikura, K.K.; Jacox, M.E. Experimental and ab initio study of the infrared spectra of ionic species derived from and trapped in solid neon. *J. Chem. Phys.* **1998**, *108*, 8381–8393. [[CrossRef](#)]
33. Wilken, S.; Johansson, P.; Jacobsson, P. Infrared spectroscopy of instantaneous decomposition products of LiPF₆-based lithium battery electrolytes. *Solid State Sci.* **2012**, *225*, 608–610. [[CrossRef](#)]
34. Lekgoathi, M.D.S.; Vilakazi, B.M.; Wagener, J.B.; Le Roux, J.P.; Moolman, D. Decomposition kinetics of anhydrous and moisture exposed LiPF₆ salts by thermogravimetry. *J. Fluor. Chem.* **2013**, *149*, 53–56. [[CrossRef](#)]